Supporting Information

Potassium-Escaping Balances Degree of Graphitization and Pore Channel Structure in Hard Carbon to Boost Plateau Sodium Storage Capacity

Niubu LeGe, Ying-Hao Zhang, Wei-Hong Lai, Xiang-Xi He, Yun-Xiao Wang, Ling-fei Zhao, Min Liu, Xingqiao Wu*, Shu-Lei Chou**

Precursor preparation

Gourds are purchased from Taobao website, and extracting seeds but retaining the shells. Subsequently, processed the shells into powder without washing step, aiming to investigate the effects of potassium on the structure evolution of HC. Moreover, a comparative analysis by subjecting a portion of the gourd powder to a washing procedure using purified water. The process involved mixing 20 g of powder with 200 ml of purified water, stirring for 720 minutes, filtering the mixture, and subsequently drying it in an oven at 80℃ for 720 minutes. Energy-dispersive spectroscopy (EDS) results indicate that potassium is the third-highest element (1.5 wt.%) in the primitive gourd only to carbon and oxygen, which can be effectively removed by a washing process (Figure S1) and table S1. Additionally, the ash-forming element residual are also calculated by burning the HCs in open air up to 800 ℃ in a muffle furnace (Table S1).

Details of the CTS

To synthesis each HCs, we employed 800 mg of gourd powder, molding it into cylindrical forms through a press. The setup of carbothermal shock as shown in Figure S2. Before initiating CTS, evacuating the apparatus to a vacuum level of 30 torr. Throughout the CTS process, the cylindrical precursor was positioned between two graphite sheets, and ensuring continuous vacuum operation (Figure S2a). Employing an ultra-fast heating rate of 50°C/s, the precursor was heated to 2800°C and maintained for 20 seconds, followed by cooling down to room temperature within a minute. Figure S2b, c depicts a comparison of precursor before and after CTS, revealing complete carbonization of the precursor.

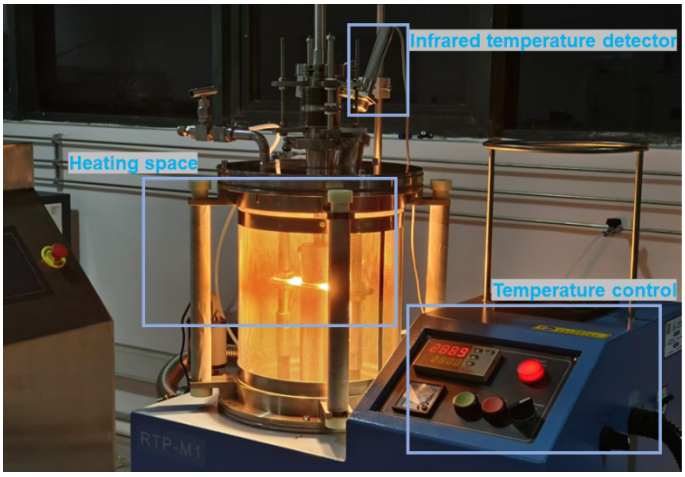

Figure S1. The photograph of carbothermal shock equipment.

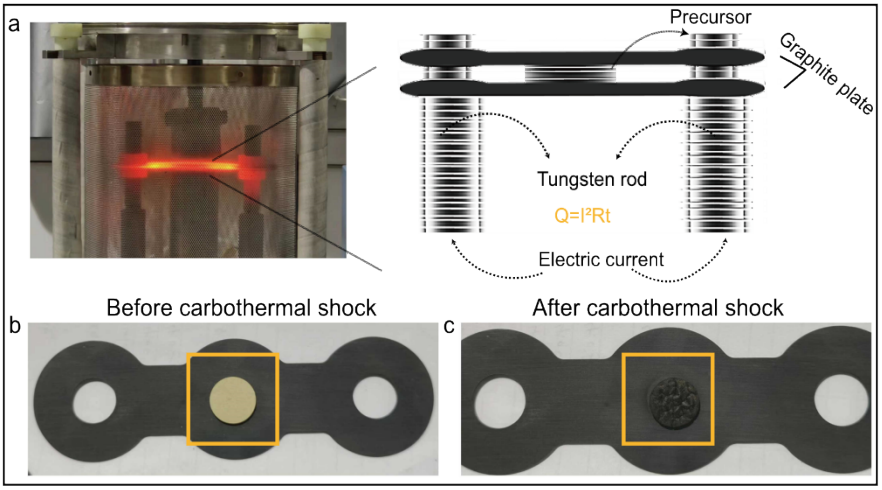

Figure S2. An overview of carbothermal shock. a) showcasing the graphite plates sandwiched with the precursor visibly reaching a bright red state. The operational principle of the Joule-heating device relies on the passage of electric current through two tungsten rods, generating high temperatures through resistive heating effects. These elevated temperatures are then transferred to the upper and lower graphite plates, subsequently transmitted

through these plates to the precursor sandwiched in between. The precursor, in close proximity to the graphite plates, undergoes the heating effects of high temperatures, initiating sintering and carbonization processes, ultimately leading to the synthesis of hard carbon. b) and c) 2 comparative photographs vividly depicting the condition of precursor after undergoing carbothermal shock, exhibiting complete carbonization.

Details of the TFH

As a point of comparison, a conventional TFH method also employed to heat the gourd to 1400°C, got a HC named G-TFH1400. The powder was placed within a graphite container, and subjecting it to a tubular furnace, then underwent heating in a nitrogen (N_2) atmosphere at a rate of 5 ℃/min until reaching 1400 ℃, where it was held for a duration of 120 minutes.

Preparation of the working electrode

Prepare the slurry in a weight ratio of HC: Super P: Sodium Alginate (2%) = 80:10:10. Use a surgical blade to evenly coat the slurry onto a copper foil. Vacuum dry the coated foil in an oven at 90℃ for 12 hours. Cut the dried foil into 10 mm circular electrode pieces, and weigh them before placing them in a glove box for further use. The loading amount of active material on the working electrode within the range of 1.1-1.3 mg/cm^2.

Assembly of the half-cell

Assemble the working electrode into Na||HC(PB) half-cell (CR-2032). Sodium metal foil is used as the counter electrode. All assembly steps are conducted inside an argon-filled glove box with water and oxygen content below 0. 1 ppm. Glass fiber (GF/A, Whatman, UK) is used as the separator. The electrolyte is prepared by dissolving 1 M $NaPF_6$ in DEGDME.

Electrochemical testing

Galvanostatic charge-discharge tests at room temperature are conducted using a Neware battery test system (CT-4008T, Shenzhen, China). The voltage range is set from 0 to 2.0 V. Galvanostatic intermittent titration technique (GITT) testing is performed using a Neware battery test system (CT-4008T, Shenzhen, China) with a pulse current of 20 mA/g in the voltage range of 0-2.0 V for 30 minutes, with a rest interval of 4 hours.

Assembly and testing of the full cell

Prussian blue is widely regarded as a promising cathode material for sodium-ion batteries, $Na_2MnFe(CN)_6$, a typical Prussian blue-type cathode material, is presented with its XRD pattern in Figure S17a. $Na_2MnFe(CN)_6$ was used as the cathode to assess the practicality of our G-CTS2800,applied onto aluminum foil in a weight ratio of active material to super P to Sodium Alginate (2 wt.%) of 80:10:10. All assembly steps are conducted inside an argon-filled glove box

with water and oxygen content below 0. 1 ppm. Glass fiber (GF/A, Whatman, UK) is utilized as the separator, and the voltage range is configured from 1.6V to 3.8V. The electrolyte is purchased from Wenzhou NaTech New Energy Technology Co., Ltd. The initial Galvanostatic discharge/charge curves of $Na_2MnFe(CN)_6$ in a sodium half-cell, presented in Figure S17b, demonstrate a high reversible capacity of 151.7 mAh/g and an ICE of 98.8%.

Structural Characterization

X-ray powder diffraction (XRD) analyses were performed using a Tongda TD-3500 X-ray powder diffractometer with Cu-Kα radiation operating at 40 kV and 30 mA. The morphology of HC was observed using a CIQTEK SEM3100 scanning electron microscope (SEM) equipped with an energy-dispersive X-ray spectroscope. Raman spectra were obtained using a LabRAM JY-HR 800 spectrometer with a 532 nm laser. The crystal structure was investigated using high-resolution TEM (HR-TEM) imaging on an FEI Tecnai G2 F20 transmission electron microscope. XPS analysis was carried out using a Thermo Scientific K-Alpha spectrometer with an Al Kα X-ray source to examine the surface chemical state. The pore structure information was acquired through nitrogen adsorption/desorption measurements using a Micromeritics ASAP 2460 volumetric gas adsorption apparatus at 77 K. Small-angle X-ray scattering (SAXS) experiments were conducted using an Xeuss instrument (xenocs, France) with an enclosed Cu receiving target (λ = 1.54 Å) and a Pilatus 3R 300K detector. Inductively coupled plasma optical emission spectrometry (ICP-OES) tests were conducted using an Agilent ICP-OES 5110.

Calculating Energy density (Wh/kg)

$$E = \frac{Q_P \times m_P \times V}{m_N + m_P} \tag{S1}$$

Where: Q_P is the specific capacity based positive anode (mAh/g). m_P is the active mass of positive anode (mg). m_N *is* active mass of negative anode (mg). V is the discharge voltage at plateau.

Calculating diffusion coefficient of sodium ions (D_{Na+}) from GITT

According to the simplified form of Fick's second law, the diffusion coefficient of sodium ions (D_{Na+}) can be calculated using the formula S2. The formula is as follows:

$$D_{Na+} = \frac{4}{\pi\tau}\left(\frac{m_B V_M}{M_B S}\right)^2\left(\frac{\Delta E_S}{\Delta E\tau}\right) \tag{S2}$$

Where: τ is the pulse time. S is the active surface area of the HC electrodes (cm^2). m_B (g) is the active mass of HC electrodes. M_B (g/mol) is the molar mass of HC (g/mol).V_M (cm^3/mol) is the molar volume of HC. ΔE_S (V) is the voltage change caused by the current pulse. $\Delta E\tau$ is the voltage change during galvanostatic discharge/charge.

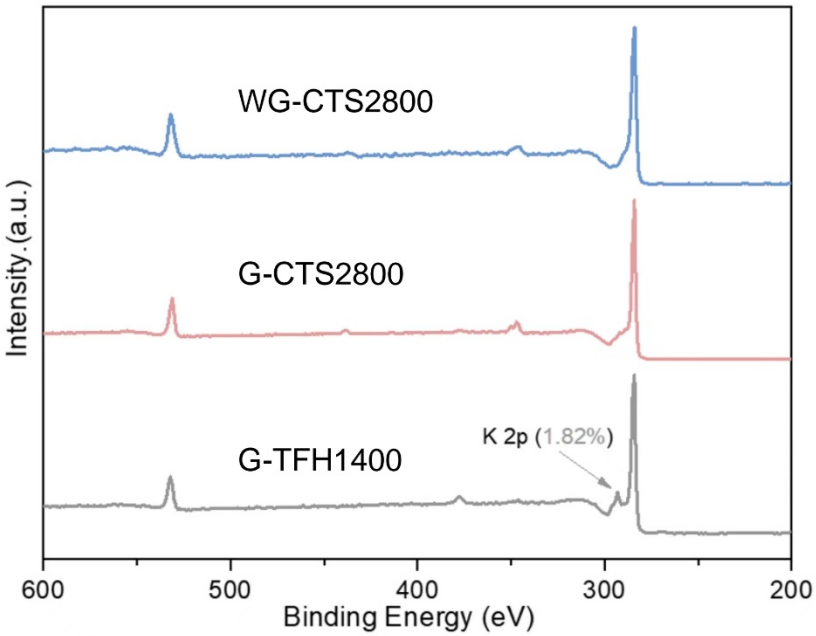

Figure S3. XPS patterns to analysis element differences, various HCs of G-TFH1400, G-CTS2800 and WG-CTS2800.

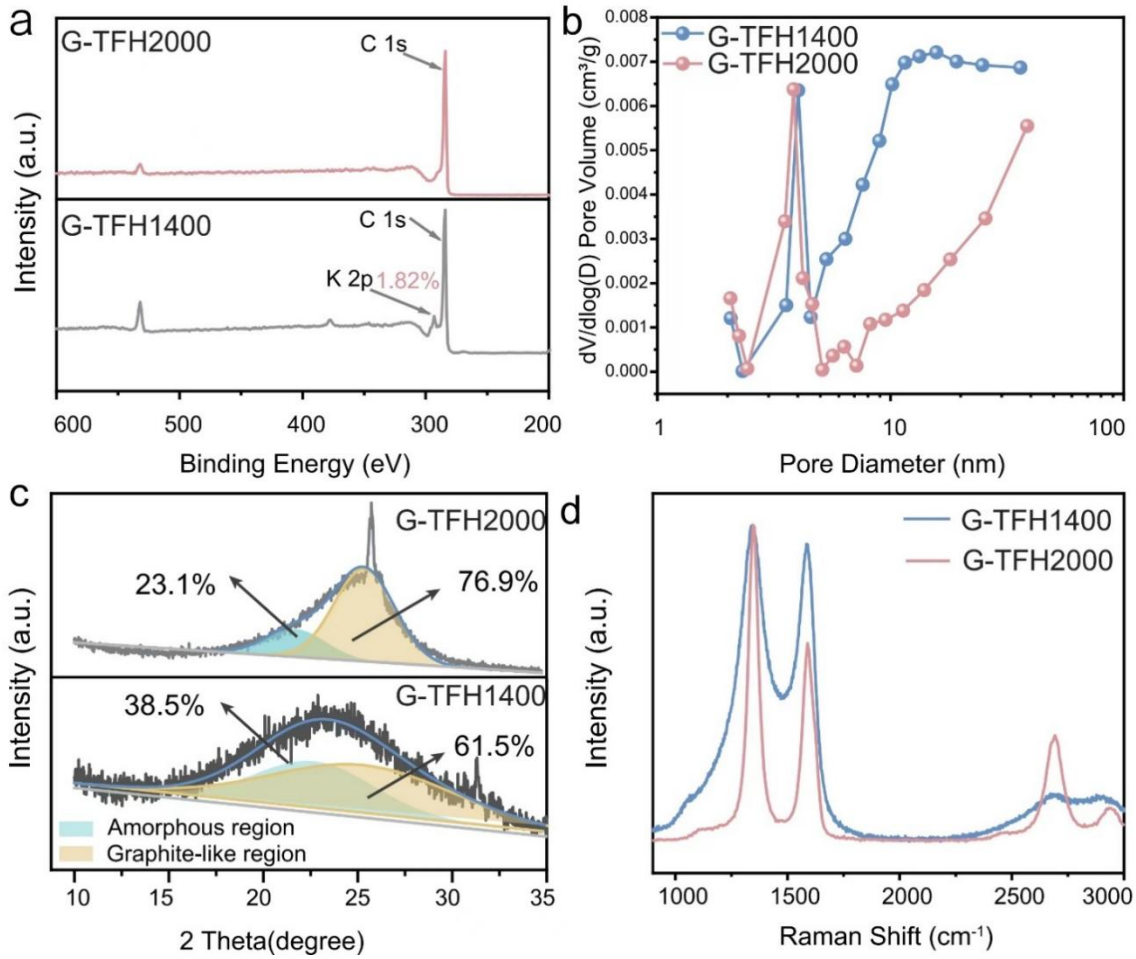

Figure S4. A structural comparison for G-TFH1400 and G-TFH2000. The analysis encompassed a) XPS patterns. b) pore size distribution determined through the BJH method. c) the division of the broadened peak of (002) of XRD into two regions: the amorphous region and the graphite-like region. and d) Raman spectra.

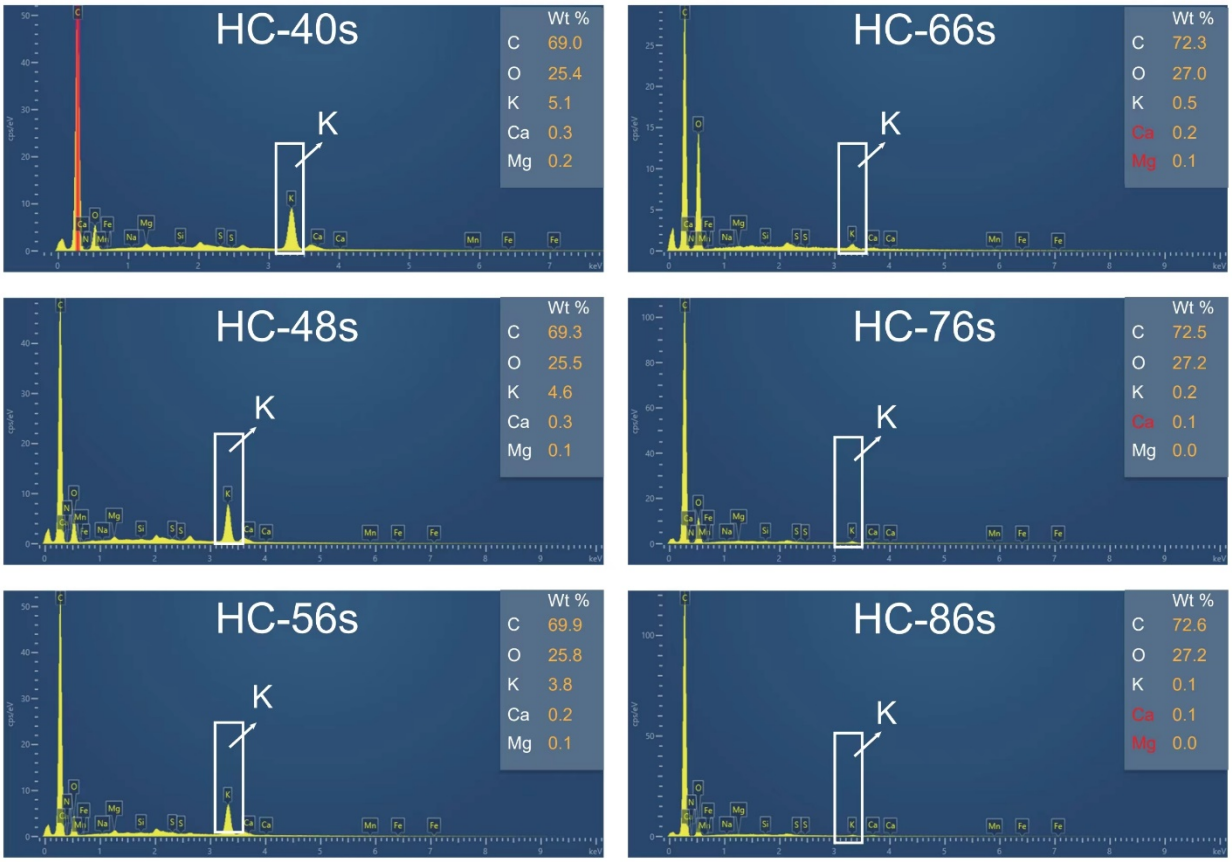

Figure S5. A change pattern about the element variation in an *ex-situ* CTS process at different carbonization time, including HC-40s, HC-48s, HC-56s, HC-66s, HC-76s, and HC-86s.

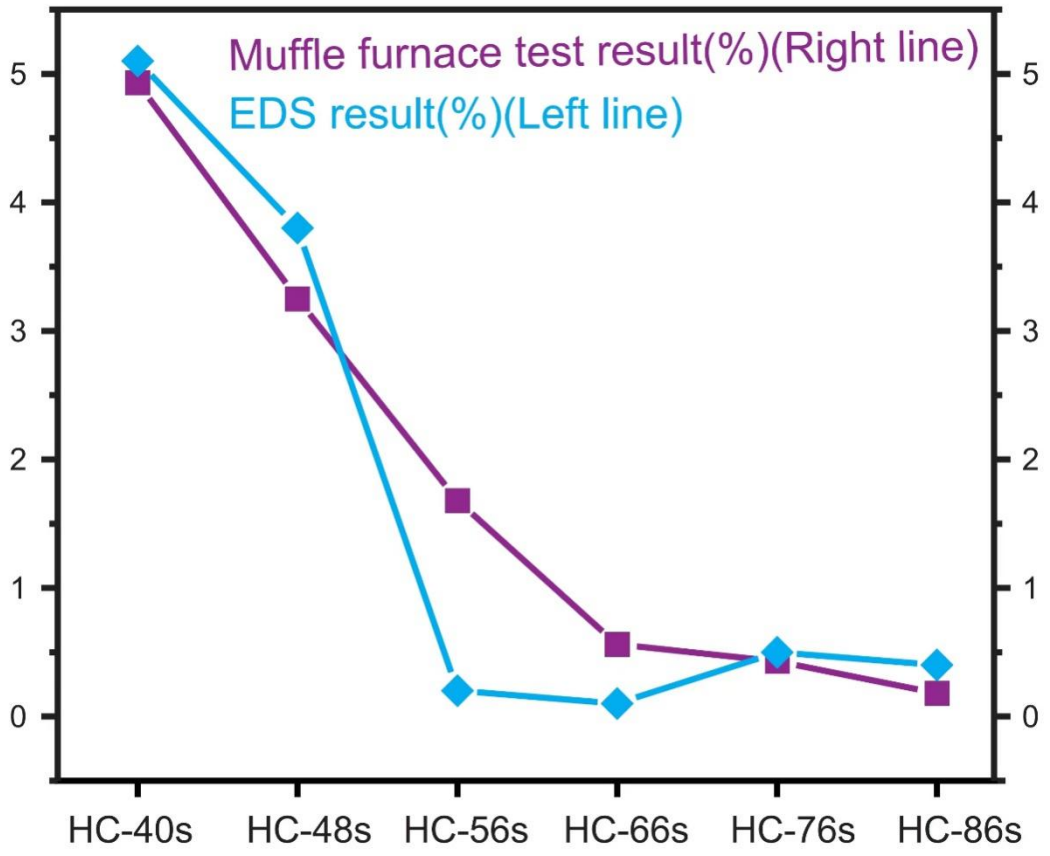

Figure S6. A change pattern about the element variation from precursor to hard carbon in an *ex-situ* CTS process at different carbonization time. The change in ash-forming element residual (the data got by burning the HCs in open air to 800℃ in muffle furnace) and K residual (the data from EDS).

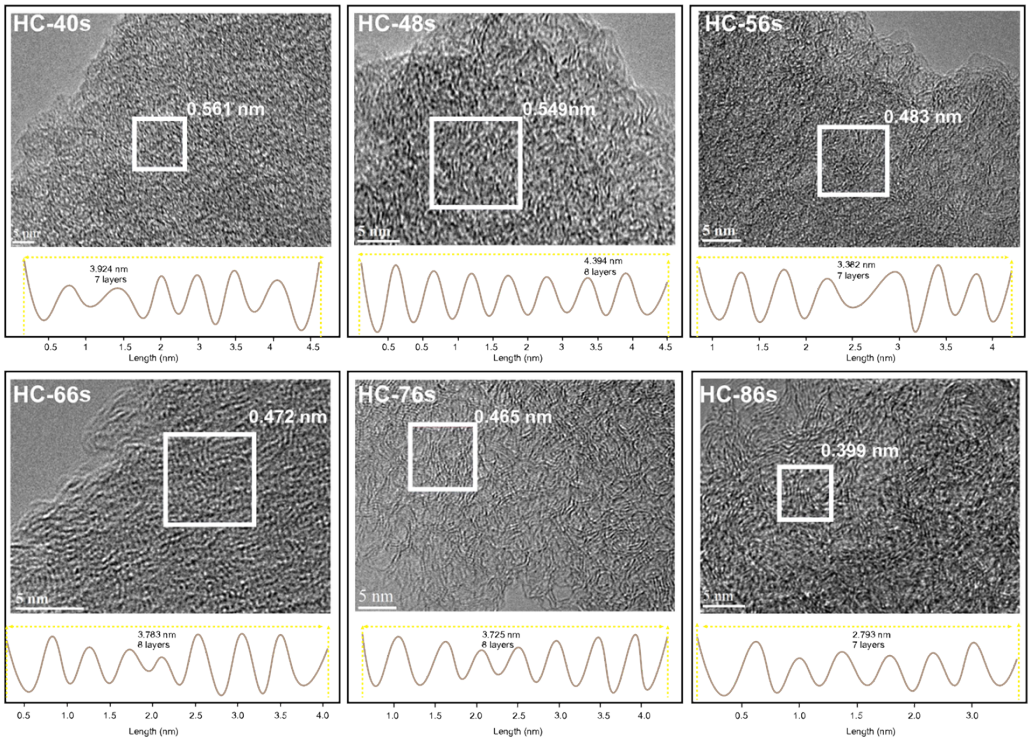

Figure S7. HRTEM pattern of the HCs varies from time in an *ex-situ* CTS process at different carbonization time, including HC-40s, HC-48s, HC-56s, HC-66s, HC-76s and HC-86s.

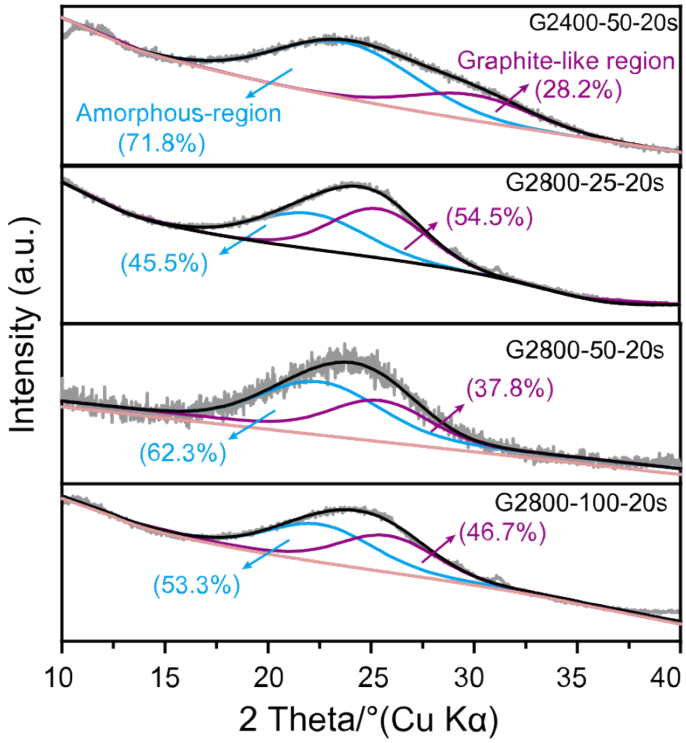

Figure S8. The broad XRD peak of (002) as divided into two regions: amorphous region and graphite-like region.

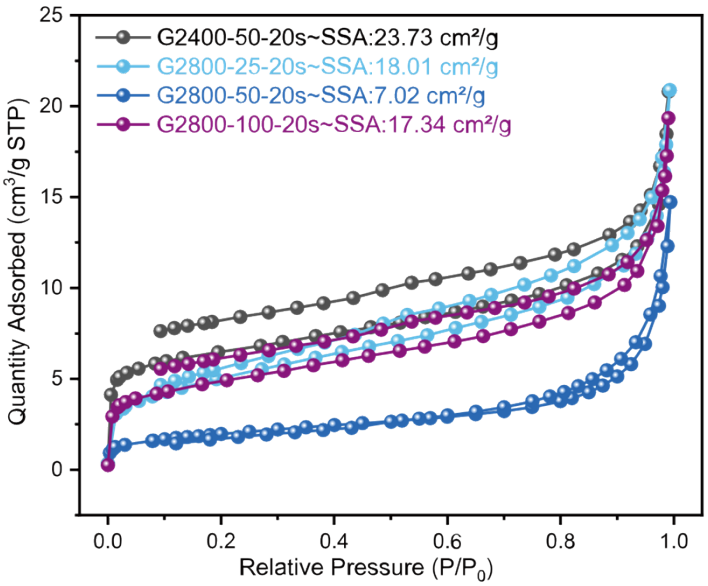

Figure S9. N_2 adsorption/desorption isotherms.

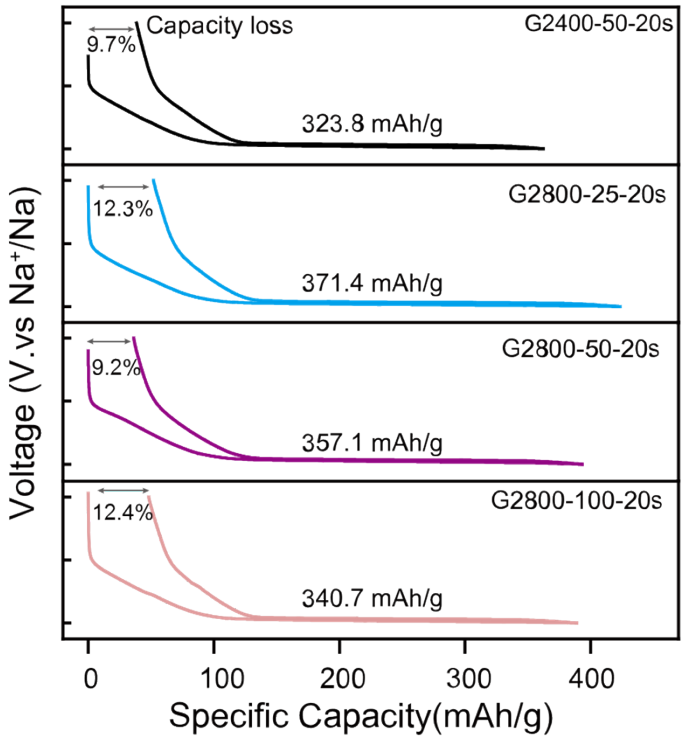

Figure S10. Galvanostatic initial discharge/charge curves at 50 mA/g.

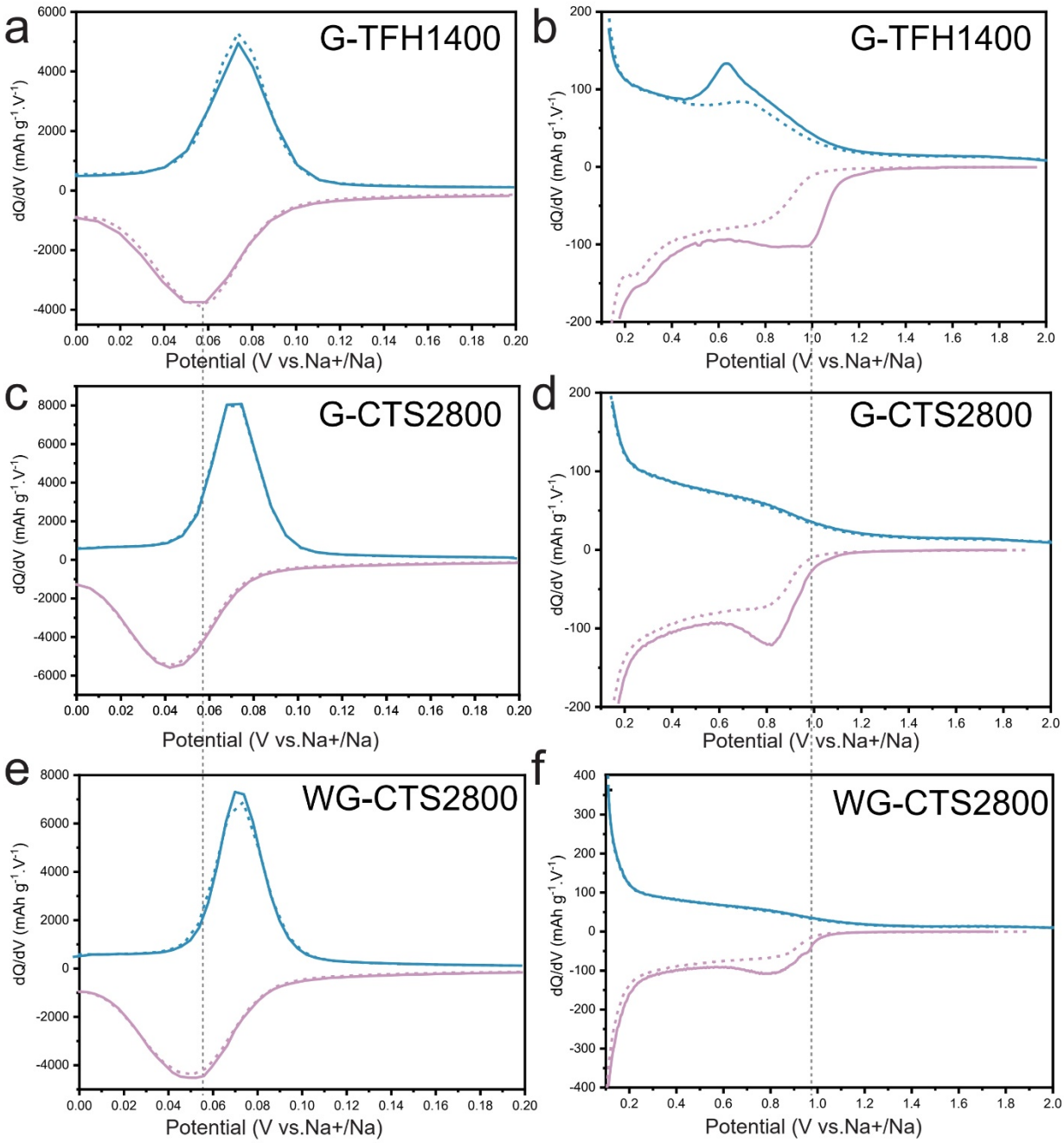

Figure S11. A pattern about dV/dQ-V curve. a), c) and e) dV/dQ-V curves in a voltage range of 0.0-0.2 V at current densities of 50 mA/g. b), d) and f) dV/dQ-V curves in a voltage range of 0.1-0.2 V at current densities of 50 mA/g.

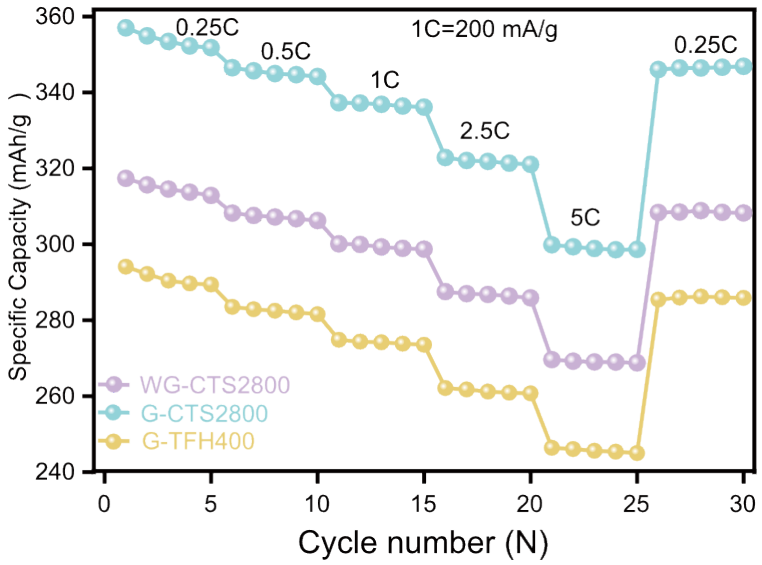

Figure S12. Rate performance test result of G-TFH1400, G-CTS2800 and WG-CTS2800 in half-cell.

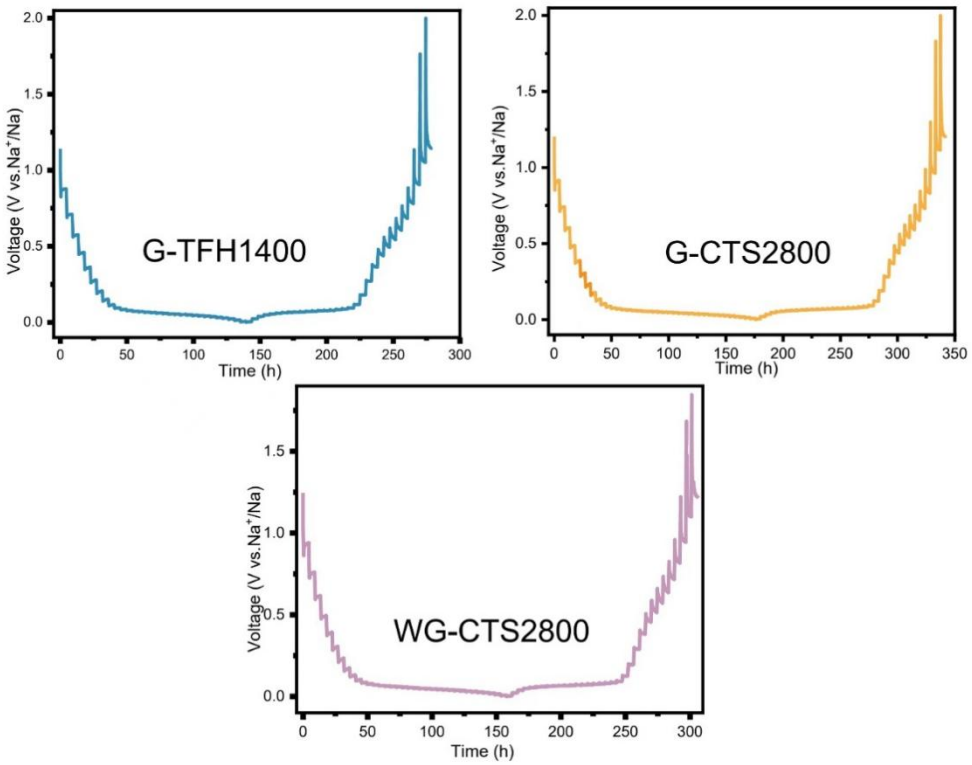

Figure S13. GITT curve of G-TFH1400, G-CTS2800 and WG-CTS2800.

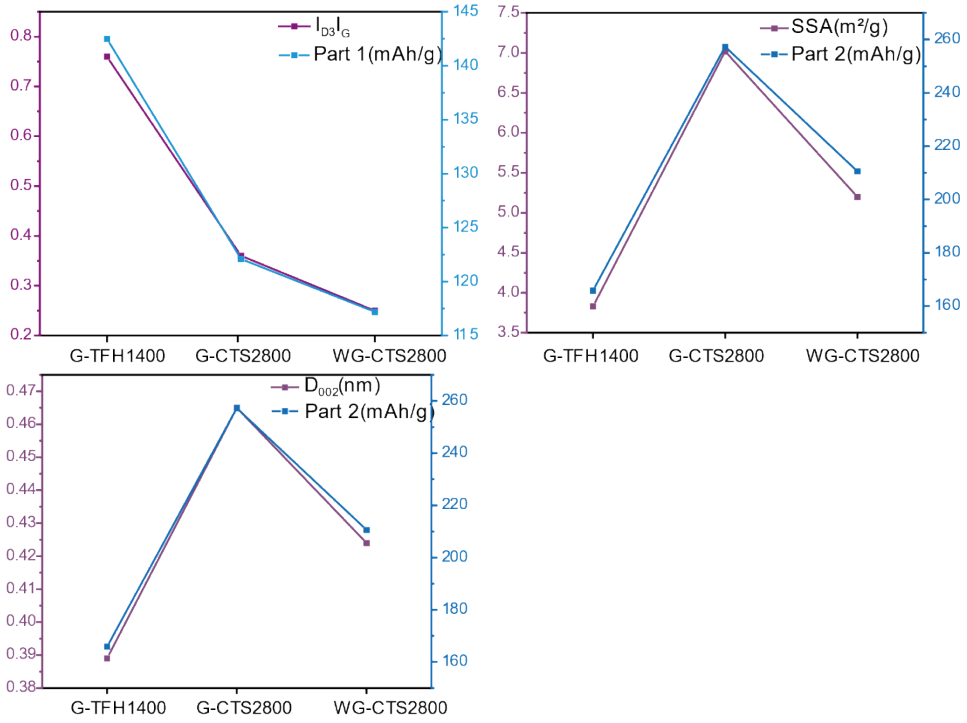

Figure S14. A relationship between microstructure parameters with sodium storage capacity in different region.

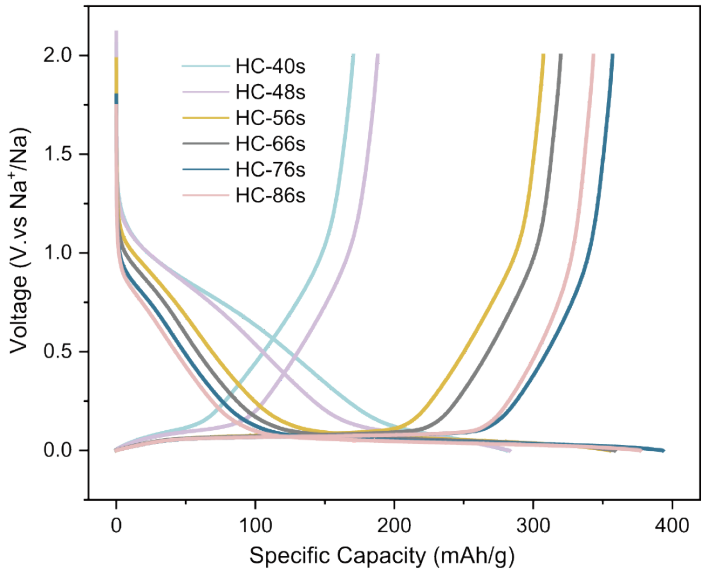

Figure S15. Galvanostatic initial discharge/charge curves at 50 mA/g.

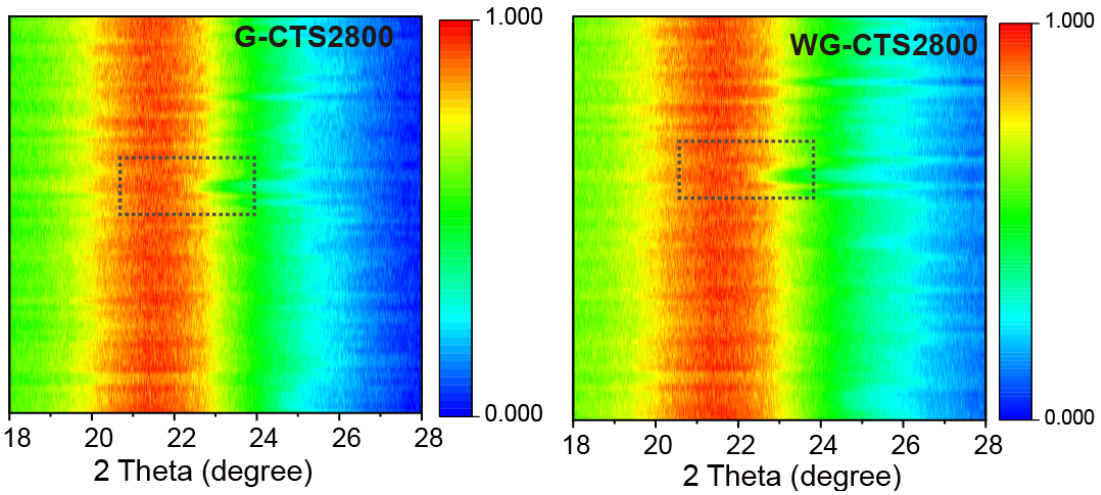

Figure S16. The *in-situ* XRD patterns. of G-CTS2800 and WG-CTS2800 during the initial discharge/charge process at 20 mA/g.

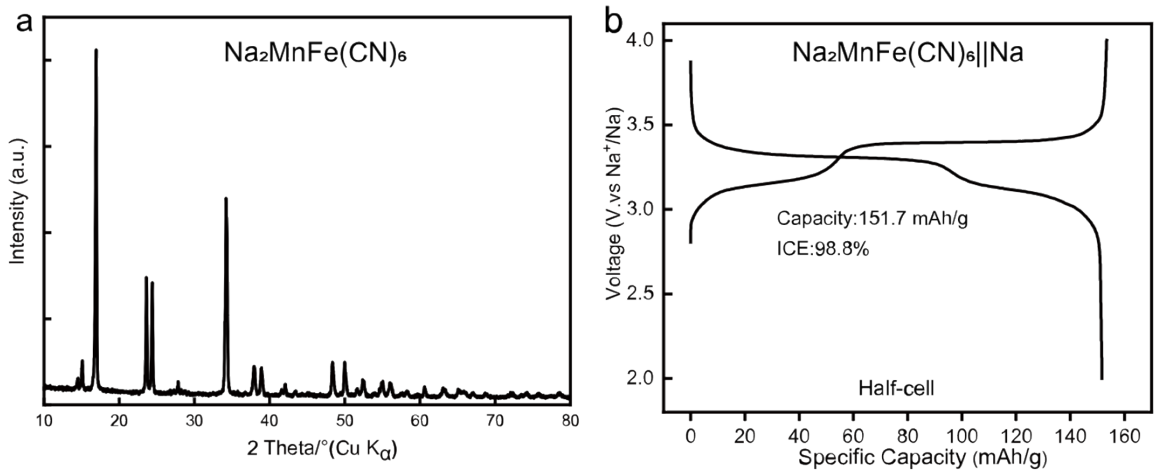

Figure S17. (a) XRD pattern of $Na_2MnFe(CN)_6$. (b) the initial Galvanostatic discharge/charge curves of $Na_2MnFe(CN)_6$ in sodium half-cell at 50 mA/g.

Table S1. The potassium content that calculated by different technologies.

HCs	ash [a] (wt. %)	ash reduction (wt. %)	Potassium content [b] mg/Kg	Potassium reduction mg/Kg
Primitive-gourd powder	**5.3**	**--**	**19390.6**	**--**
Washed-gourd powder	**1.41**	**--**	**4172.2**	**--**
G-TFH1400	**1.31**	**3.99**	**5084.7**	**14305.9**
G-CTS2800	**0.43**	**4.87**	**737.8**	**18652.8**
WG-CTS2800	**0.18**	**1.23**	**617.1**	**3555.1**

[a] The results were obtained through an ash-forming element test method, wherein the HCs was exposed to air and subsequently incinerated in a muffle furnace at 800°C for a period of 10 hours, in order to acquire the ash reduction from precursor to HCs.
[b] The potassium content was obtained through inductively coupled plasma optical emission spectrometry (ICP-OES).

Table S2. Some basic parameters on HCs vary from heating temperature and holding time.

HCs	D_{002} (nm)	ash (wt. %)	Ash reduction (wt. %)	SSA (m^2/g)	Pore volume (cm^3/g)	Plateau capacity (mAh/g)
Primitive-gourd	--	5.3	--	--	--	--
HC-40s	0.561	4.93	0.37	1.0712	0.006597	41.13
HC-48s	0.549	3.25	2.05	2.3329	0.006289	57.7563
HC-56s	0.483	1.68	3.62	8.3604	0.017283	190.9545
HC-66s	0.472	0.56	4.74	8.1957	0.021116	213.4245
HC-76s	0.465	0.43	4.87	7.0279	0.022362	260.2399
HC-86s	0.399	0.18	5.12	10.5538	0.024174	256.8224

Table S3. The influence of heating rate and holding time on the structure and properties of GTS Samples.

Materials	Reversible capacity (mAh/g)	Ash-residual (%)	SSA (cm^2/g)	Graphite-like region (%)	Synthesis time (s)
G2400-50-20s	323.8	4.21	23.73	21.2	68
G2800-25-20s	371.4	4.95	18.01	54.5	132
G2800-50-20s	357.1	4.87	7.02	37.6	76
G2800-100-20s	340.7	4.28	17.34	46.7	48

Table S4. The comparation for the sodium storage performance of HC in ether electrolyte that have been reported in the literature.

HCs	Synthesizing Time	Capacity (mAh/g)	ICE (%)	Current density (mA/g)	Electrolyte	Reference
G-CTS2800	76 seconds	357.1	90.8	50	1M $NaPF_6$ in DEGDME	This work
PCS@V@C	> 24 hours	216.7	85.3	100	1M $NaPF_6$ in DEGDME	[1]
GH5-1000	> 24 hours	302.5	70.3	50	1M $NaPF_6$ in Diglyme	[2]
HC-0.2P-1000	> 21 hours	328.5	68.3	50	1M $NaPF_6$ in Diglyme	[3]
H-1500	> 14 hours	390	~70.9	50	1M $NaPF_6$ in Dimethyl	[4]
M11005	>5 mins	299.4	88.9	30	1M $NaPF_6$ in DEGDME	[5]
MPC-1000	>5 hours	319	71	20	1M $Na_2CF_3SO_3$ in Diglyme	[6]
HCP	>7 hours	338.2	91.2	20	1M $Na_2CF_3SO_3$ in Diglyme	[7]
Al_2O_3-P6M-5	>6 hours	~175	70.2	100	1M $Na_2CF_3SO_3$ in Diglyme	[8]

References

1 D. Cheng, Z. Li, M. Zhang, Z. Duan, J. Wang and C. Wang, *ACS Nano*, 2023, **17**, 19063.

2 Man Yuan, Chenyang Meng, Ang Li, Bin Cao, Yue Dong, Dengke Wang, Xuewei Liu, Xiaohong Chen and Huaihe Song, *Small*, 2022, **18**, 2105738.

3 Xiuping Yin, Yufeng Zhao, Xuan Wang, Xiaochen Feng, Zhixiu Lu, Yong Li, Hongli Long, Jing Wang, Jinyan Ning and Jiujun Zhang, *Small*, 2022, **18**, 2105568.

4 Z. Tang, R. Zhang, H. Wang, S. Zhou, Z. Pan, Y. Huang, D. Sun, Y. Tang, X. Ji, K. Amine and M. Shao, *Nature communications*, 2023, **14**, 6024.

5 Y. Zhen, Y. Chen, F. Li, Z. Guo, Z. Hong and M.-M. Titirici, *Proceedings of the National Academy of Sciences*, 2021, **118**, e2111119118.

6 J.-L. Xia, D. Yan, L.-P. Guo, X.-L. Dong, W.-C. Li and A.-H. Lu, *Adv. Mater.*, 2020, **32,** 2000447.

7 B.-H. Hou, Y.-Y. Wang, Q.-L. Ning, W.-H. Li, X.-T. Xi, X. Yang, H.-j. Liang, X. Feng and X.-L. Wu, *Adv. Mater.*, 2019, **31,** 1903125.

8 Q. Lin, J. Zhang, D. Kong, T. Cao, S.-W. Zhang, X. Chen, Y. Tao, W. Lv, F. Kang and Q.-H. Yang, *Adv. Energy Mater.*, 2019, **9**, 1803078.